This is a repository copy of *Determination of absorption coefficients in AlInP lattice matched to GaAs*.

White Rose Research Online URL for this paper:
http://eprints.whiterose.ac.uk/91100/

Version: Accepted Version

Article:

Cheong, J.S., Ng, J.S., Krysa, A.B. et al. (2 more authors) (2015) Determination of absorption coefficients in AlInP lattice matched to GaAs. Journal of Physics D: Applied Physics, 48 (40). 5101. ISSN 0022-3727

https://doi.org/10.1088/0022-3727/48/40/405101

Reuse
Unless indicated otherwise, fulltext items are protected by copyright with all rights reserved. The copyright exception in section 29 of the Copyright, Designs and Patents Act 1988 allows the making of a single copy solely for the purpose of non-commercial research or private study within the limits of fair dealing. The publisher or other rights-holder may allow further reproduction and re-use of this version - refer to the White Rose Research Online record for this item. Where records identify the publisher as the copyright holder, users can verify any specific terms of use on the publisher's website.

Takedown
If you consider content in White Rose Research Online to be in breach of UK law, please notify us by emailing eprints@whiterose.ac.uk including the URL of the record and the reason for the withdrawal request.

eprints@whiterose.ac.uk
https://eprints.whiterose.ac.uk/

Determination of absorption coefficients in AlInP lattice matched to GaAs

J. S. Cheong, J. S. Ng, A. B. Krysa, J. S. L. Ong[1] and J. P. R. David
Department of Electronic and Electrical Engineering, University of Sheffield, Mappin Street, S1 3JD, U.K.
[1]Currently at School of Microelectronic Engineering, University Malaysia Perlis, 02600, Malaysia.

Abstract— The absorption properties of $Al_{0.52}In_{0.48}P$ have been investigated near the fundamental absorption edge by measuring the photocurrent as a function of wavelength in a series of PIN and NIP diodes. Modelling of the photocurrent in these structures enables the absorption coefficients to be determined accurately over a wide dynamic range, which allows the direct and indirect band-gap to be determined.

Index Terms— absorption coefficient, AlInP, bandgap, Urbach tail, photocurrent

I. Introduction

The ternary alloy $Al_{0.52}In_{0.48}P$ (AlInP thereafter) has received great attention recently for various optoelectronic applications. Being the widest bandgap III-V semiconductor material which can be grown lattice-matched to GaAs, AlInP is used in various devices such as multi-junction solar cells [2], visible lasers [3], multi-quantum barrier lasers [4] and laser diodes [5]. More recently, it has been used for demonstrating a narrow band high sensitivity photodiode [6] and avalanche photodiode [7] working at ~ 480 nm. In several of these devices, to optimize their performance requires an accurate knowledge of the material absorption coefficient, α as a function of wavelength near the optical band-edge. Although Kato et al. [1] showed that the optical properties of AlInP over a broad wavelength range of 225-1033 nm can be deduced from ellipsometry measurements, the noise around the fundamental absorption in the dielectric spectra results in unreliable absorption coefficients in the wavelength range of 440 – 550 nm where $\alpha < 10^5$ cm^{-1}.

A broad range of absorption coefficients from 10^6 down to 10^0 cm^{-1} is usually obtained by merging the data from both transmission and ellipsometry measurements [8-10]. However, such data has not been reported for AlInP. In this paper, we show that α can be determined accurately over a wide dynamic range in a wavelength range of 380 – 550 nm via spectral response measurements on a series of PIN and NIP diodes.

II. Device Growth, Fabrication and Characterization

Three AlInP PINs and one NIP homo-junction diode with nominal intrinsic layer thickness, w of 1.0, 0.8, and 0.2 µm were grown by low pressure (150 Torr) metalorganic-vapor phase epitaxy (MOVPE) in a horizontal flow reactor at 680-730 ºC on n^+ (p^+) GaAs substrates, which have an off-cut angle of 10º towards [111A] plane to minimize the copper-platinum (Cu-Pt) ordering [11]. The epilayers were capped with heavily doped ~50 nm thin GaAs to ensure a good ohmic contact. Conventional alkyls and hydrides were used for the epitaxial growth, with zinc (TMZ) and silicon (silane) used as p and n-type dopants respectively.

Double X-ray rocking curves reveals that the compressive lattice mismatch of AlInP in all our structures compared to GaAs is minimal at $< 6 \times 10^{-4}$, with a nominal aluminum composition of 52.3%. To ensure that the incident light is absorbed by only the AlInP, the GaAs cap of the optical window is etched off in the devices as shown in Fig. 1 using wet chemical etching. The central top 1.0 µm AlInP cladding in some devices was further thinned using Inductive Couple Plasma (ICP) to give p^+ cladding thicknesses of 0.2 – 0.5 µm ± 0.07 as tabulated in Table I. Finally, mesa diodes of 35 – 210 µm radii were formed for optical and electrical characterization.

Capacitance-voltage (C-V) measurement was performed on the mesa diodes to determine w and the doping densities in p^+-i-n^+ layers (N_p, N_i and N_n respectively). Secondary Ions Mass spectroscopy (SIMs) measurements were undertaken on several of the structures to corroborate these parameters, as well as obtaining thicknesses of the cladding p^+ (n^+) layers. Although results from both measurements agree on the values of w and N_i, the p^+ claddings doping densities estimated from C-V and SIMs were estimated to be 3-4$\times10^{17}$ and 1×10^{18} cm^{-3} respectively. One possible reason for this discrepancy may be due to hydrogen passivation of acceptors which represents a common problem in MOVPE grown wide bandgap III-V semiconductors such as GaN [12]. Background oxygen contamination [13] and the solubility of the zinc dopants in AlInP [14] can also decrease the concentration of the active Zn acceptors. Conversely, it was reported that high carrier concentration of $>10^{18}$ cm^{-3} can be achieved using Si-dopant

TABLE I
DEVICE PARAMETERS OF AlInP DIODES

Layer	p^+ (n^+) thickness (µm)	w (µm)	N_p (x10^{17} cm^{-3})	N_n (x10^{17} cm^{-3})	N_i (x10^{15} cm^{-3})
P1	1.00	0.97	4.0	20	2
P2-1	1.00	1.12	2.0	10	15
P2-2	0.47				
P2-3	0.23				
P3-1	1.00	0.25	4.3	20	16
P3-2	0.26				
N1-1	1.00	0.81	2.5	20	2
N1-2	0.42				
N1-3	0.27				

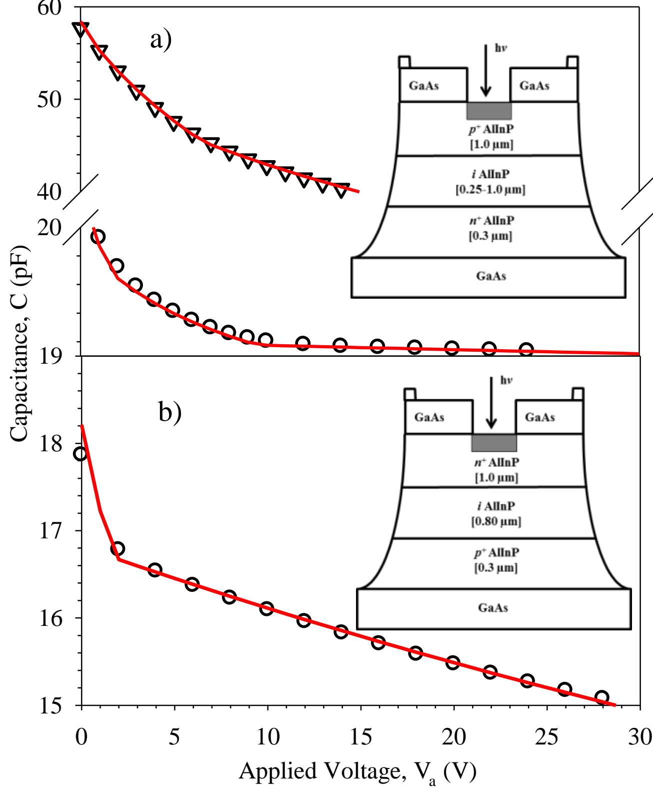

Fig. 1 Measured (symbols) and modelled (lines) capacitance of the a) PINs (P2-1 and P3-1 as ○ and ▽respectively) and b) N1-1. Also shown in the inset is the schematic diagram of the device structures, with RIE-etched area shaded in grey.

[13]. Assuming the doping densities in the n^+ and p^+ regions are 1-2×10^{18} and 2-5×10^{17} cm^{-3} respectively as shown in Table I the results obtained from C-V modelling (with a dielectric constant of 11.25, interpolated from InP and AlP values), showed good agreement with the experimental data as showed in Fig. 1.

III. Results and Discussion

A 100 W tungsten halogen bulb and a grating monochromator which has a resolution of ± 1.5 nm were used to measure the spectral responses of the 200 µm radii devices as shown in Fig. 2. Since the dark current at low bias voltages is extremely low in these devices [15], very small photocurrents (~10 pA) around the cut-off wavelength regime where the absorption is expected to be very weak, can still be measured accurately. The results were confirmed using phase sensitive technique where the light signal was mechanically modulated and the photocurrent was measured using a lock-in amplifier. The quantum efficiencies (QE) of the devices illustrated in Fig. 2 were deduced from a calibrated silicon photodiode and were confirmed using a 442 nm He-Cd laser, where the laser beam was focused to a ~20 µm diameter spot on the device optical windows.

The measured photocurrent from a p^+-i-n^+ structure consists of i) minority electrons diffusing from the p^+ layer to the depletion region, ii) electron-hole pairs generated within the depletion region, and iii) minority holes diffusing from the n^+ layer to the depletion region. The associated internal QEs' (η_p, η_i and η_n) correspond to these photocurrent components (ie. i to iii) and can be expressed as (1) – (3) as shown at the bottom of the page where L_e (L_h), D_e (D_h) and S_e (S_h) are diffusion lengths, diffusion coefficients and surface recombinations respectively [16]. X_1 and X_2 are the distance from the top surface to the depletion edge in the p^+ and n^+ region respectively whereas X_3 is the total thickness of the p^+-i-n^+ layers. All carriers generated in the depletion region were assumed to contribute to the photocurrent. The external QE of a p^+-i-n^+ structure, η can be written as

$$\eta = R(\eta_p + \eta_i + \eta_n). \quad (4)$$

where the reflectivity, R as a function of wavelength, λ is related to the refractive index, n and extinction coefficient, k, given by

$$R(\lambda) = \frac{[n(\lambda)-1]^2 + k^2(\lambda)}{[n(\lambda)+1]^2 + k^2(\lambda)}. \quad (5)$$

k is related to α via $k = \frac{\alpha\lambda}{4\pi}$.

The refractive index, n of AlInP reported in [1] covers the wavelength range of interest so was used to estimate R.

$$\eta_p = \left[\frac{\alpha L_e}{\alpha^2 L_e^2 - 1}\right]\left[\frac{\frac{S_e L_e}{D_e} + \alpha L_e - \exp(-\alpha X_1)\left(\frac{S_e L_e}{D_e}\cosh\left(\frac{X_1}{L_e}\right) + \sinh\left(\frac{X_1}{L_e}\right)\right)}{\frac{S_e L_e}{D_e}\sinh\left(\frac{X_1}{L_e}\right) + \cosh\left(\frac{X_1}{L_e}\right)} - \alpha L_e \exp(-\alpha X_1)\right] \quad (1)$$

$$\eta_i = (\exp[-\alpha X_1])(1 - \exp[-\alpha(X_2 - X_1)]) \quad (2)$$

$$\eta_n = \left[\frac{\alpha L_h}{\alpha^2 L_h^2 - 1}\right][\exp[-\alpha(X_3 - X_2)]]\left[\alpha L_h - \frac{\frac{S_h L_h}{D_h}\left[\cosh\left(\frac{X_3}{L_h}\right) - \exp(-\alpha X_3)\right] + \sinh\left(\frac{X_3}{L_h}\right) + \alpha L_h \exp(-\alpha X_3)}{\frac{S_h L_h}{D_h}\sinh\left(\frac{X_3}{L_h}\right) + \cosh\left(\frac{X_3}{L_h}\right)}\right] \quad (3)$$

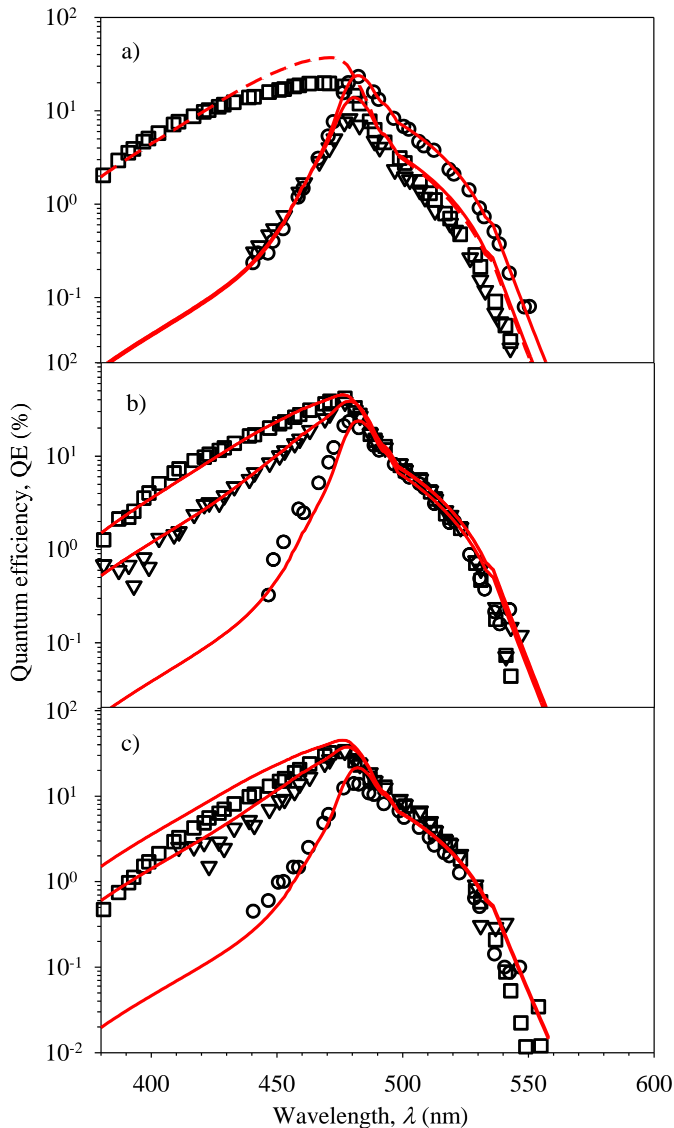

Fig. 2 Experimentally obtained QE (symbols) from a) P1, P3-1 and P3-2 shown as ○, ▽ and □ respectively. b) P2-1 and P2-2 and P2-3 shown as ○, ▽ and □ respectively. c) N1-1 and N1-2 and N1-3 shown as ○, ▽ and □ respectively. Simulated results are shown in lines.

The parameters L_e (L_h) can be independently obtained by measuring the change in responsivity under illumination of 442 nm as a function of reverse bias voltage before the onset of avalanche multiplication. This measurement was performed on those samples with a 1.0 μm thick top cladding (ie. P1, P2-1, P3-1 and N1-1) since > 99.9% of the photons are absorbed in the top cladding layer and therefore the photocurrent contribution due to the intrinsic region and bottom cladding layer can be neglected. The increasing photocurrent with applied bias voltage is due to the depletion into the top cladding layer and therefore enables us to estimate the minority carrier diffusion length [17]. Using an initial value α of ~ 1×10^5 cm^{-1} at 442 nm [1] and μ_e of 160 $cm\ s^{-1}$ [18], L_e determined from the PINs was 0.155 μm ± 0.015. Due to the short L_e, the modelled results showed insignificant change when surface recombination velocities (assuming $S_e = S_h$) and were increased from the nominal values of 1×10^7 $cm\ s^{-1}$ [19].

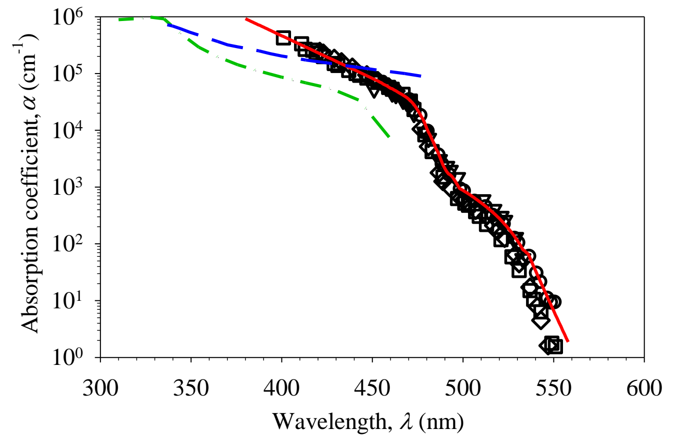

Fig. 3 Absorption coefficient, α obtained from P1, P2-1, P3-1 and N1-1 as ○, ▽, □, and ◇ respectively. The highest achievable α for a given wavelength (solid line) was taken as the bulk value. The published AlInP [1] and GaP [12] data are shown as dashed, dashed-dot-dot and dashed-dot lines respectively.

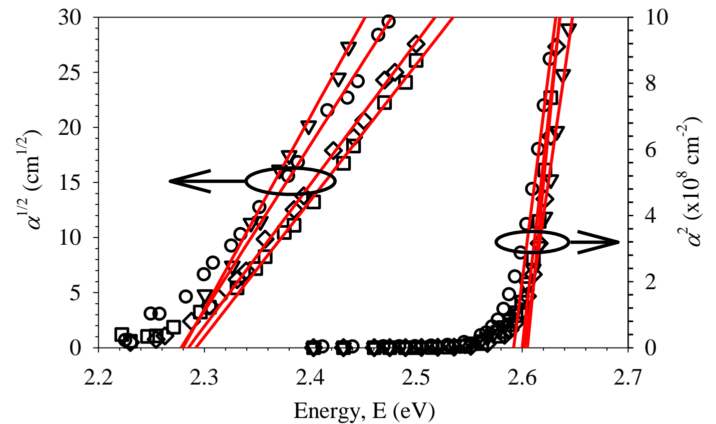

Fig. 4 Experimentally obtained root (left) and square (right) of absorption coefficient obtained from P1, P2-1, P3-1 and N1-1 at 0 V shown as ○. ▽,□ and ◇ respectively. The fittings are shown as lines to extract the indirect (left) and direct energy gaps (right).

Similar measurement was done on N1-1 giving L_h of 0.170 μm ± 0.015, using μ_h of 10 $cm\ s^{-1}$ [18].

After determining the parameters in (1) – (3), α can be solved numerically by fitting the modelled QE to the experimental results. α shown in Fig. 3 extracted from P1, P2-1, P3-1 and N1-1 are in close agreement, assuming L_e and L_h of 0.155 and 0.170 μm respectively. This suggests that the measured α is independent of the doping type for the levels used in this work, in agreement with those reported in other semiconductors [20, 21].

AlInP is an indirect-gap semiconductor and to understand the behavior of α with wavelength, we need to determine the energy gaps. To extract the band-gap of AlInP, $\alpha^{1/2}$ versus photon energy extracted from P1, P2-1, P3-1 and N1 at 0 V are plotted as shown in Fig. 4. These data can be fitted by straight lines and by extrapolating these to the x-intercept, E_g which corresponds to the X-valley was found to be 2.289 ± 0.006 eV. The direct gap, E_Γ was estimated to be 2.597 ± 0.008 eV using similar method by plotting α^2 versus photon energy. These results are comparable to those obtained from photoluminescence or cathodoluminescence spectroscopy [22, 23] which give E_g and E_Γ of 2.26 – 2.33 eV and 2.50 – 2.60

eV respectively for disordered material (reported 4 K data was converted to 300 K data by subtracting 80meV).

The discrepancy between the measured α and those reported by Kato et al. [1] are clearly shown in Fig. 3, The α determined here decreases rapidly at 470 nm and relatively more gradually at 495 nm, and this can be attributed to the absorption process in Γ and X valleys respectively. For comparison, the absorption behavior of GaP [24], also an indirect band-gap semiconductor, is also shown in Fig. 3 and is seen to be similar to our data but blue shifted by about ~ 30 nm due to the larger E_Γ of GaP, reported as 2.757 eV [25].

The α from Fig. 3 for AlInP was used to reproduce the QE's in P1-1, P2-1, P3-1 and N1-1 as illustrated in Fig. 2. Good agreements over 3 orders of magnitude can be seen in these samples. Although the peak response wavelength agrees well, the QE obtained from the experimental data are slightly lower than the modelled results in P3-1, most probably due to the presence of surface roughness or a surface oxide layer which is ignored in the simulations.

The same QE measurements were performed on the RIE-etched devices. As RIE is known to roughen the surface of semiconductor and degrade the optical performance [26], no attempt was made to extract α from these results. Instead, α was extrapolated from 400 nm to 380 nm as shown in Fig. 3 to simulate the QE obtained from these devices. The modelled results in Fig. 2 showed surprisingly good fit to the experimental data, especially in the P2 samples. The surface roughness and damage depth of ~ 100 nm after RIE etching [26] may explain the discrepancies found in the P3 and N1 samples in Fig. 2 where the surface optical transmission and minority carriers diffusion length may have been reduced.

CONCLUSION

The spectral responses of a series of AlInP PINs and NIP with different layer thicknesses were measured and from their quantum efficiency (QE), the absorption coefficients in AlInP over five orders of magnitude can be extracted accurately. In materials with relatively short diffusion lengths, this technique is found to be insensitive to the surface recombination velocity. The E_g and E_Γ in disordered AlInP are found to be 2.289 and 2.597 eV respectively. .

REFERENCE

1. Hirokazu Kato, S.A., Hiroshi Nakanishi and Kouji Ohtsuka, Optical Properties of (AlxGa1-x)0.5In0.5P Quaternary Alloys Japanese Journal of Applied Physics, 1994. **33**(1A): p. 186-192.
2. Yang, M.-J., et al., Photoluminescence analysis of InGaP top cells for high-efficiency multi-junction solar cells. Solar Energy Materials and Solar Cells, 1997. **45**(4): p. 331-339.
3. Sugawara, H., K. Itaya, and G. Hatakoshi, Characteristics of a distributed Bragg reflector for the visible-light spectral region using InGaAlP and GaAs: Comparison of transparent- and loss-type structures. Journal of Applied Physics, 1993. **74**(5): p. 3189-3193.
4. Kishino, K., et al., Enhanced carrier confinement effect by the multiquantum barrier in 660 nm GaInP/AlInP visible lasers. Applied Physics Letters, 1991. **58**(17): p. 1822-1824.
5. Atkins, C.N., et al., Low threshold room temperature GaAs/AlGaAs quantum cascade laser with InAlP waveguide. Electronics Letters, 2011. **47**(21): p. 1193-1194.
6. Yonggang, Z., et al., GaInP-AlInP-GaAs Blue Photovoltaic Detectors With Narrow Response Wavelength Width. Photonics Technology Letters, IEEE, 2010. **22**(12): p. 944-946.
7. Jeng Shiuh, C., et al., $Al_{0.52}In_{0.48}P$ SAM-APD as a Blue-Green Detector. Selected Topics in Quantum Electronics, IEEE Journal of, 2014. **20**(6): p. 142-146.
8. Dash, W.C. and R. Newman, Intrinsic Optical Absorption in Single-Crystal Germanium and Silicon at 77\ifmmode^\circ\else\textdegree\fi{}K and 300\ifmmode^\circ\else\textdegree\fi{}K. Physical Review, 1955. **99**(4): p. 1151-1155.
9. Philipp, H.R. and E.A. Taft, Optical Constants of Germanium in the Region 1 to 10 ev. Physical Review, 1959. **113**(4): p. 1002-1005.
10. Philipp, H.R. and E.A. Taft, Optical Constants of Silicon in the Region 1 to 10 ev. Physical Review, 1960. **120**(1): p. 37-38.
11. Su, L.C., I.H. Ho, and G.B. Stringfellow, Effects of substrate misorientation and growth rate on ordering in GaInP. Journal of Applied Physics, 1994. **75**(10): p. 5135-5141.
12. Amano, H., et al., P-Type Conduction in Mg-Doped GaN Treated with Low-Energy Electron Beam Irradiation (LEEBI). Japanese Journal of Applied Physics, 1989. **28**(12A): p. L2112.
13. Bertness, K.A., et al., AlInP benchmarks for growth of AlGaInP compounds by organometallic vapor-phase epitaxy. Journal of Crystal Growth, 1999. **196**(1): p. 13-22.
14. Ohba, Y., et al., A study of p-type doping for AlGaInP grown by low-pressure MOCVD. Journal of Crystal Growth, 1988. **93**(1–4): p. 613-617.
15. Ong, J.S.L., et al., Impact Ionization Coefficients in $Al_{0.52}In_{0.48}P$. Electron Device Letters, IEEE, 2011. **32**(11): p. 1528-1530.
16. Yernaux, M.I., et al., A one-dimensional model for the quantum efficiency of front-surface-field solar cells. Solar Cells, 1984. **13**(1): p. 83-97.
17. Woods, M.H., W.C. Johnson, and M.A. Lampert, Use of a Schottky barrier to measure impact ionization coefficients in semiconductors. Solid-State Electronics, 1973. **16**(3): p. 381-394.
18. Wood, S.A., et al., Electron transport in AlGaInP quantum well lasers. Applied Physics Letters, 1999. **75**(12): p. 1748-1750.
19. Bimberg, D., M. Grundmann, and N.N. Ledentsov, Quantum Dot Heterostructures. 1999: Wiley.
20. Casey, H.C., D.D. Sell, and K.W. Wecht, Concentration dependence of the absorption *coefficient for n− and p−type GaAs between 1.3 and 1.6* eV. Journal of Applied Physics, 1975. **46**(1): p. 250-257.
21. Dishman, J.M. and M. DiDomenico, Optical Absorption by Impurities in p-Type Gallium Phosphide. Physical Review B, 1971. **4**(8): p. 2621-2634.
22. Mowbray, D.J., et al., Electronic band structure of AlGaInP grown by solid-source molecular-beam epitaxy. Applied Physics Letters, 1994. **65**(2): p. 213-215.
23. Onton, A. and R.J. Chicotka, *Conduction Bands in In1−xAlxP.* Journal of Applied Physics, 1970. **41**(10): p. 4205-4207.
24. Aspnes, D.E. and A.A. Studna, Dielectric functions and optical parameters of Si, Ge, GaP, GaAs, GaSb, InP, InAs, and InSb from 1.5 to 6.0 eV. Physical Review B, 1983. **27**(2): p. 985-1009.
25. Takizawa, T., Wavelength Modulated Reflectivities of the Direct Exciton Edge in GaP. Journal of the Physical Society of Japan, 1983. **52**(3): p. 1057-1063.
26. Cheung, R., et al., Reactive ion etching induced damage in GaAs and Al 0.3 Ga 0.7 As using SiCl 4. Semiconductor Science and Technology, 1992. **7**(9): p. 1189.